

Rapid fluvial remobilization of sediments deposited by the 2021 Chamoli disaster, Indian Himalaya

Matthew J. Westoby^{1,2,*}, Stuart A. Dunning³, Jonathan L. Carrivick⁴, Thomas J. Coulthard⁵, Kalachand Sain⁶, Amit Kumar⁶, Etienne Berthier⁷, Umesh K. Haritashya⁸, David E. Shean⁹, Mohd. Farooq Azam¹⁰, Kavita Upadhyay¹¹, Michele Koppes¹², Harley R. McCourt¹, and Dan H. Shugar¹³

¹Department of Geography and Environmental Sciences, Northumbria University, Newcastle upon Tyne NE1 8ST, UK

²School of Geography, Earth and Environmental Sciences, University of Plymouth, Plymouth PL4 8AA, UK

³School of Geography, Politics and Sociology, Newcastle University, Newcastle upon Tyne NE1 7RU, UK

⁴School of Geography and water@leeds, University of Leeds, Leeds LS2 9JT, UK

⁵Energy and Environment Institute, University of Hull, Hull HU6 7RX, UK

⁶Wadia Institute of Himalayan Geology, Dehradun, Uttarakhand 248001, India

⁷Laboratoire d'Études en Géophysique et Océanographie Spatiales (LEGOS), Université de Toulouse, 31400 Toulouse, France

⁸Department of Geology and Environmental Geosciences, University of Dayton, Dayton, Ohio 45469, USA

⁹Department of Civil and Environmental Engineering, University of Washington, Seattle, Washington 98195, USA

¹⁰Indian Institute of Technology Indore, Simrol, Madhya Pradesh 453552, India

¹¹Independent journalist/researcher (disaster and development), Nainital, Uttarakhand 263001, India

¹²Department of Geography, University of British Columbia, Vancouver, British Columbia V6T 1Z4, Canada

¹³waterSHED Lab, Department of Geoscience, University of Calgary, Calgary, Alberta T2N 1N4, Canada

ABSTRACT

High-magnitude mass flows can have a pervasive geomorphological legacy, yet the short-term response of valley floors to such intense disturbances is poorly known and poses significant observational challenges in unstable landscapes. We combined satellite remote sensing, numerical modeling, and field observations to reconstruct the short-term geomorphological response of river channels directly affected by the 7 February 2021 ice-rock avalanche–debris flow in Chamoli district, Uttarakhand, India. The flow deposited $10.4 \pm 1.6 \text{ Mm}^3$ of sediment within the first 30 km and in places reset the channel floor to a zero-state condition, requiring complete fluvial re-establishment. In the 12 months post-event, $7.0 \pm 1.5 \text{ Mm}^3$ (67.2%) of the deposit volume was removed along a 30-km-long domain and the median erosion rate was $2.3 \pm 1.1 \text{ m a}^{-1}$. Most sediment was removed by pre-monsoon and monsoon river flows, which conveyed bedload waves traveling at $0.1\text{--}0.3 \text{ km day}^{-1}$ and sustained order-of-magnitude increases in suspended sediment concentrations as far as 85 km from the event source. Our findings characterize a high-mountain fluvial cascade with a short relaxation time and high resilience to a high-magnitude geomorphological perturbation. This system response has wider implications, notably for water quality and downstream hydropower projects, which may be disrupted by elevated bedload and suspended sediment transport.


INTRODUCTION

Mass movement–driven sediment cascades are hazardous to life, property, and infrastructure (e.g., Dowling and Santi, 2014) and are a key mechanism of mountain landscape evolution (e.g., Stock and Dietrich, 2003). The nature

of individual mass-flow elements is well studied (e.g., Mergili et al., 2017; Geertsema et al., 2022), but the manner in which flow deposits are remobilized and the sediment flux response remain poorly understood. This knowledge gap needs addressing due to the relationship between mass-flow activity and climate change (e.g., Chiarle et al., 2021; Zheng et al., 2021), the uncertain role of mass flows in the geological record (Bovis and

Jakob, 1999; Toby et al., 2022), and the impacts that elevated post-event sediment loads can have for hydropower projects (HPPs; Li et al., 2021) and ecosystems (e.g., Danehy et al., 2011).

On 7 February 2021, $\sim 27 \text{ Mm}^3$ of glacier ice and bedrock detached from Ronti Peak (6063 m), Chamoli district, Uttarakhand, India (Fig. 1), and transitioned into a debris flow then to a debris-laden flood along the Rishiganga–Dhauliganga–Alaknanda rivers (Shugar et al., 2021; Tiwari et al. 2022). The flow caused >200 fatalities and severely damaged key roads, bridges, and HPP installations—one under-construction (520 MW) and one operational (13.2 MW) HPP, with estimated damages to HPP infrastructure totaling $\sim \$200$ million USD (Dutta, 2021). The flow caused extensive geomorphic work (Fig. 2) including widespread channel infill as much as 100 m thick (Shugar et al., 2021), scour of hillslopes 200 m above the valley floor, temporary damming of tributary valleys, and exacerbated slope instability at Raini village, prompting rehabilitation (UDRP-AF, 2021). Rapid field reconnaissance identified dewatering debris drapes and proto-channels incising into new deposits (Fig. 2; Fig. S2 in the Supplemental Material¹). Qualitative analysis of

Matthew J. Westoby  <https://orcid.org/0000-0002-2070-5580>
*matt.westoby@plymouth.ac.uk

¹Supplemental Material. Additional methodological detail, field photographs, and modeling outputs. Please visit <https://doi.org/10.1130/GEOL.S.23686479> to access the supplemental material, and contact editing@geosociety.org with any questions.

CITATION: Westoby, M.J., et al., 2023, Rapid fluvial remobilization of sediments deposited by the 2021 Chamoli disaster, Indian Himalaya: *Geology*, v. XX, p. , <https://doi.org/10.1130/G51225.1>

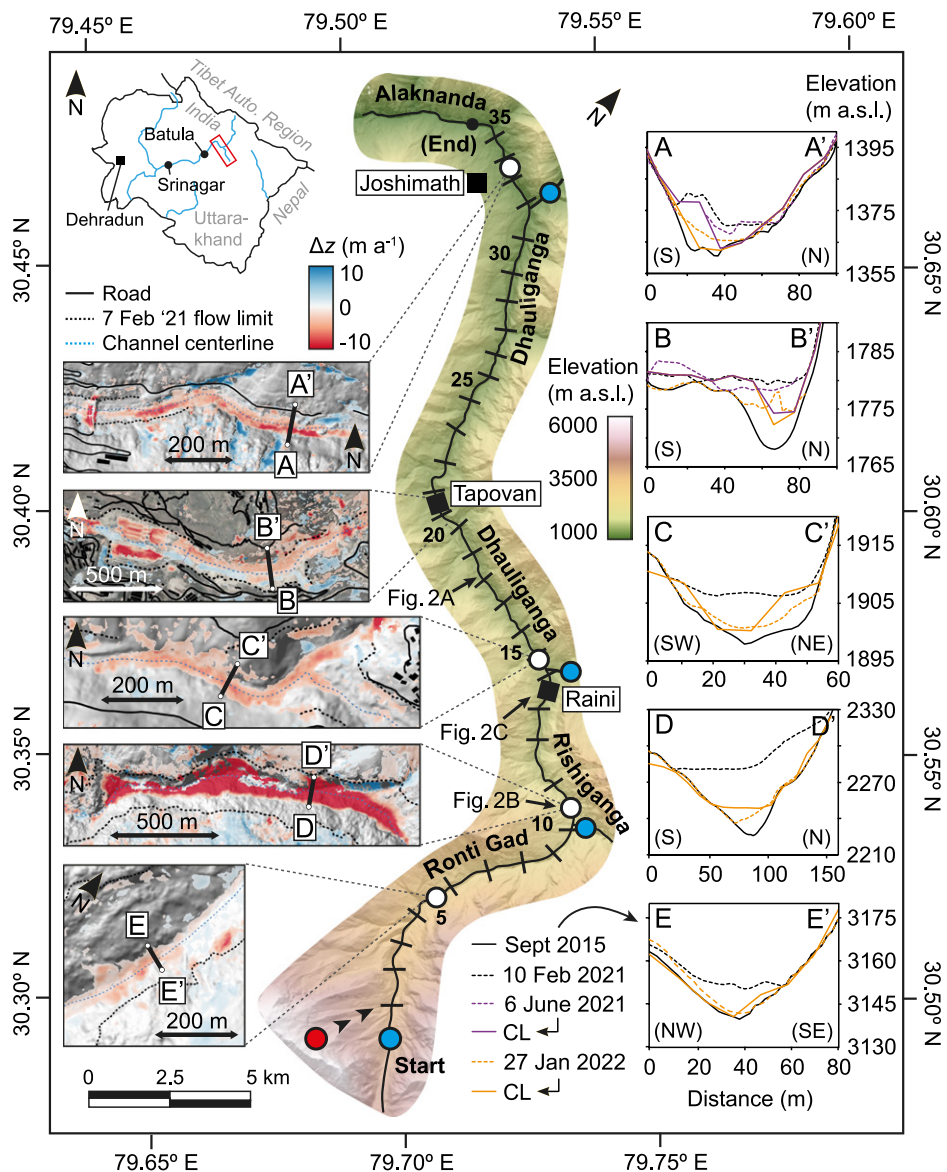


Figure 1. Geomorphological adjustment toward a pre-disturbance fluvial condition following the 7 February 2021 mass flow, Chamoli district, Uttarakhand, India. Central map shows the study domain with river names labeled, and breakpoints supporting geomorphological analysis (e.g. Fig. 4) are shown as cross hatches along the main channel (black line). Blue circles show flow discharge input locations for CAESAR-Lisflood (CL) modeling. Red circle and arrows show source location and travel direction of the rock-ice avalanche. Left panels show spatially distributed vertical change (Δz) from satellite DEM differencing (10 February 2021–27 January 2022). Right panels show cross-channel surface profiles from satellite and CL DEMs. a.s.l.—above sea level.

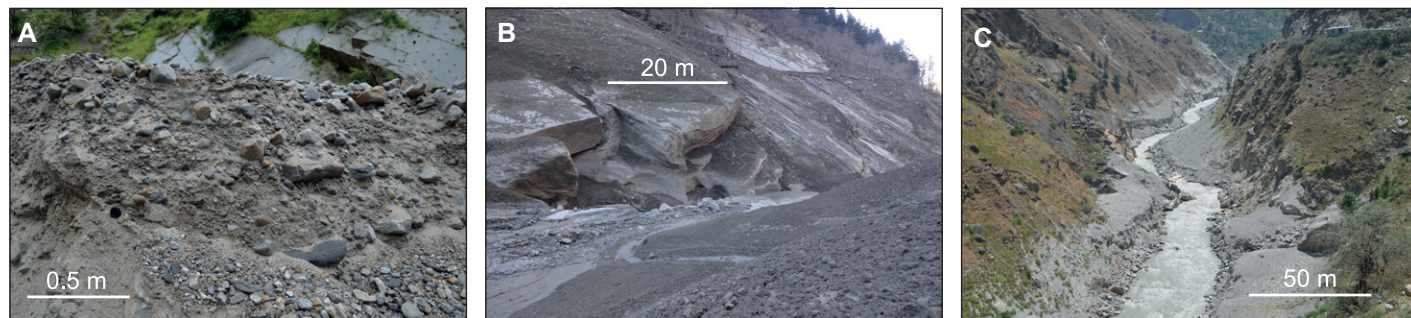


Figure 2. Post-event field photographs of the flow path. (A) New debris-flow deposits exhibiting a wide grain-size distribution including an abundance of large clasts (25% >0.08 m diameter, median grain size [D_{50}] 0.03 m). (B) Remobilizing flood deposits in the Rishiganga, view downstream. (C) Perched deposits on the Rishiganga, view upstream. Photos were taken on 8 July 2021, 19 March 2022, and 11 June 2022, respectively, by author Kumar. See Figure 1 for locations.

sediment deposited by the flow reveals clasts ≥ 64 mm supported by a fine-grained matrix that may constitute as much as 50% by volume (Fig. S3), in contrast to pre-event channel-floor sediments, which likely comprised coarse alluvium without a supporting matrix (Fig. S4). We quantify the short-term geomorphological response of the 7 February 2021 mass flow by conducting a fluvial morphodynamic assessment for ~ 1 yr post-event (10 February 2021–27 January 2022). By reconstructing post-event geomorphological adjustment and sediment yields (Figs. 3 and 4), we deliver new quantitative insights into fluvial recovery following an intense landscape-scale perturbation.

METHODS

A comprehensive description of our methods and their primary limitations is found in the Supplemental Material. Volumetric change on the valley floor was established from a 2 m satellite digital elevation model (DEM) of difference (DoD; 10 February 2021–27 January 2022, 2σ error = ± 1.1 m). We generated high-temporal-resolution (daily) detail of fluvial erosion and deposition using the hydrodynamic-landscape evolution model CAESAR-Lisflood (Coulthard et al., 2013; Fig. 3), permitting novel insights into fast-acting erosive processes and their relationship to river discharge; CAESAR-Lisflood can simulate a wide range of flows, erosion, and deposition for as many as nine grain sizes, suspended and bedload sediment transport, and failure of unstable slopes. We specified boundary conditions and parameters including DEMs representing bedrock and surface topography, an input discharge time series for all rivers entering the model, and grain-size information. Due to a lack of local flow measurements, we drove CAESAR-Lisflood using reanalysis-derived streamflow predictions (<https://geoglows.ecmwf.int>). Flow was routed across the 10 February 2021 DEM, resampled to a 10 m grid to improve computational efficiency while preserving the ability to simulate channel adjustment at a scale appropriate to the aim of the study. We used a satellite DoD for 10 February 2021–25

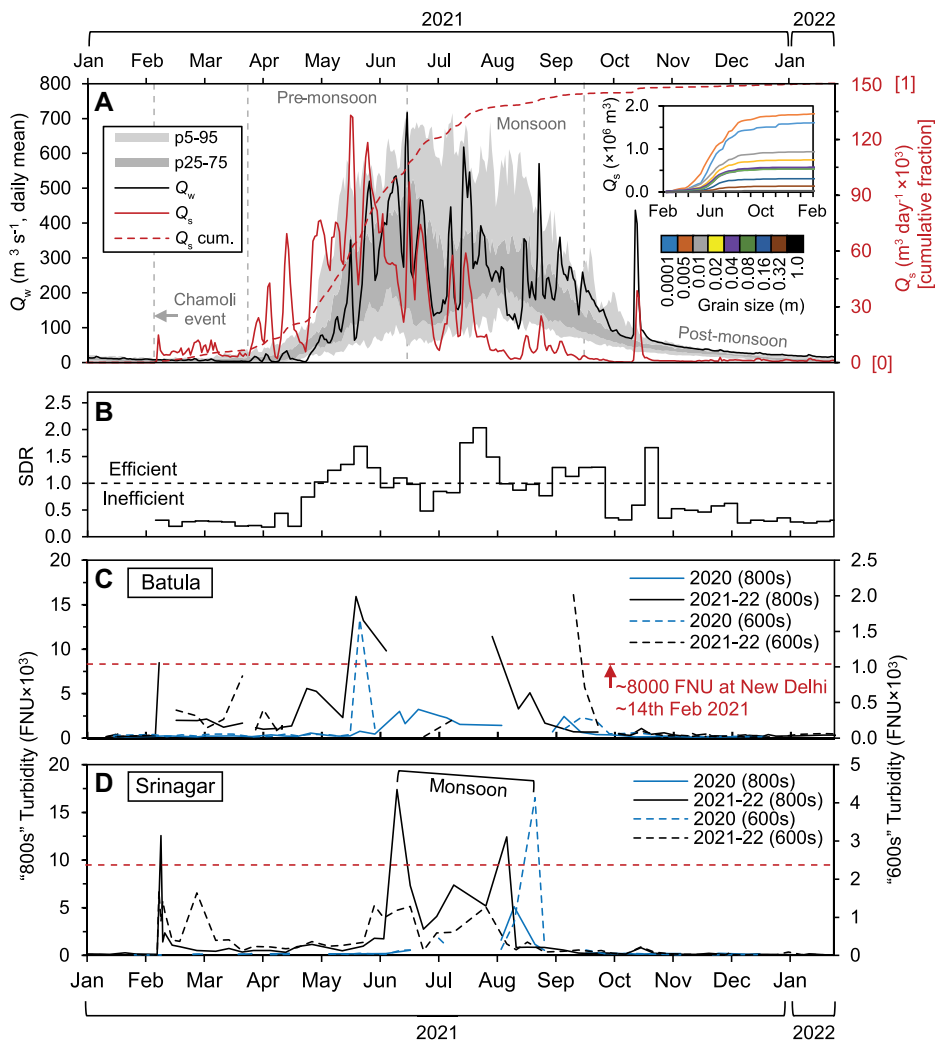


Figure 3. Modeled hydrological (water discharge, Q_w) and sediment output (Q_s) dynamics at Joshimath for the first ~12 months post-flood. (A) Daily reanalysis-derived Q_w and historical (1970–2021) percentile (p5–95) and interquartile (p25–75) Q_w ranges, and modeled Q_s from CAESAR-Lisflood. Inset shows absolute cumulative Q_s for individual grain-size fractions. (B) Modeled sediment delivery ratio (SDR). (C, D) Remote sensing-derived turbidity in the Alaknanda River at Batula and Srinagar (Fig. 1), extracted from 650 to 682 nm (“600s”) and 846–888 nm (“800s”) wavelength ranges. FNU—formazin nephelometric units.

December 2021 (2σ error = ± 1.1 m) to calibrate the model, and for analysis, we subdivided the study area into a series of geomorphological “segments.” In the absence of field observations of sediment export, the timing and relative magnitude of modeled suspended-sediment export was validated with in-channel turbidity estimates retrieved from short-temporal-repeat satellite imagery for locations 25 km (Batula) and 85 km (Srinagar) downstream of the study area (Fig. 1).

RESULTS

Post-Event Erosion and Deposition from DEM Differencing

Overall, 67.2% of sediment deposited along the primary flow pathway was removed in the first 12 months; 7.0 ± 1.5 Mm³ was removed from a 10.4 ± 1.6 Mm³ deposit. Of the removed volume, 66% was sourced from a thick (mean

36.4 m) deposit located immediately downstream of the Ronti Gad–Rishiganga confluence (Fig. 2A). The median DoD-derived erosion rate for this period was 2.3 ± 1.1 m a⁻¹. The Dhauliganga River, between Raini and Tapovan (Figs. 2B and 2C), experienced a median erosion rate of 2.2 ± 1.1 m a⁻¹. High erosion rates (mean 2.8 m a⁻¹) on the valley floor in the vicinity of the damaged Tapovan Vishnugad HPP were driven by fluvial action, while other elevation change was artificial (berm reconstruction). Downstream of Tapovan, the mean incision rate was 3.2 m a⁻¹ and as much as 10 m a⁻¹ locally at Joshimath (Fig. 1).

Rapid Erosion and Remobilization of Flow Deposits

Morphodynamic modeling with CAESAR-Lisflood shows 6.4 Mm³ net volume loss, consistent with the satellite DoD analysis (-8.7%

difference). However, at the segment scale, there were differences between the model and DoD results (Fig. 4B). From CAESAR-Lisflood modeling, we quantified four sediment discharge (Q_s) phases: (1) immediately post-event (early February–late March), (2) pre-monsoon (late March–mid-June), (3) summer monsoon (mid-June–mid-September), and (4) post-monsoon (mid-September onward) (Fig. 3A).

Immediately post-event, the mean erosion rate was 2.4 m a⁻¹, and 4% of the new sediment was evacuated. At this time, the system remained inefficient, with a sediment delivery ratio (SDR; a measure of sediment transport efficiency) of ~ 0.3 as channels re-established (Fig. 3B). The pre-monsoon phase was characterized by short-lived, high-magnitude sediment export, predominantly of fines (Fig. 3A); sediment export accounted for 62% (4.3×10^6 m³) of annual Q_s , and the mean erosion rate was 5.3 m a⁻¹. This phase also saw a switch to an efficient, albeit short-lived, hydro-geomorphic system (SDR > 1). Peak Q_s (13.2×10^4 m³ day⁻¹) occurred in mid-May, preceding peak water discharge (Q_w) by one month.

During the summer monsoon, exhaustion of fine-grained sediment, perhaps compounded by bed armoring and the development of perched deposits due to rapid incision (e.g., Fig. 2C, Fig. S4B), markedly reduced Q_s while Q_w remained high (Fig. 3A). The falling limb of the Q_s curve occurred primarily in this period, during which total Q_s was 1.8×10^6 m³ (mean erosion rate 2.0 m a⁻¹) or 26% of the cumulative annual load. The remaining 4% of annual Q_s was exported in the post-monsoon phase (mean erosion rate 0.7 m a⁻¹), when SDR reduced to < 1 . During 17–19 October, Uttarakhand experienced unseasonably heavy rainfall (Rawat et al., 2022). The consequent rapid rise in sediment transport was resolved by CAESAR-Lisflood (Fig. 3A), triggering a short-lived increase in sediment transport efficiency (Fig. 3B; SDR = 1.7) that is evident in our independent turbidity analyses (Figs. 3C and 3D).

The CAESAR-Lisflood morphodynamic modeling enables us to reconstruct complex and transient spatio-temporal patterns of post-event erosion and deposition (Fig. 4C). Some valley segments have long periods when they are primarily erosional or depositional, and we clearly observed the passage of at least three sediment waves with a velocity of 0.1 – 0.3 km day⁻¹. The waves initiated in segments 1, 10, and 20 and were most active from mid-March (week 6; pre-monsoon) to late August (week 25; monsoon).

Suspended Sediment Transport

The initial event produced a sudden and extreme increase in turbidity (Figs. 3C and 3D). We detected a maximum of 12,500 FNU (formazin nephelometric units) at Srinagar,

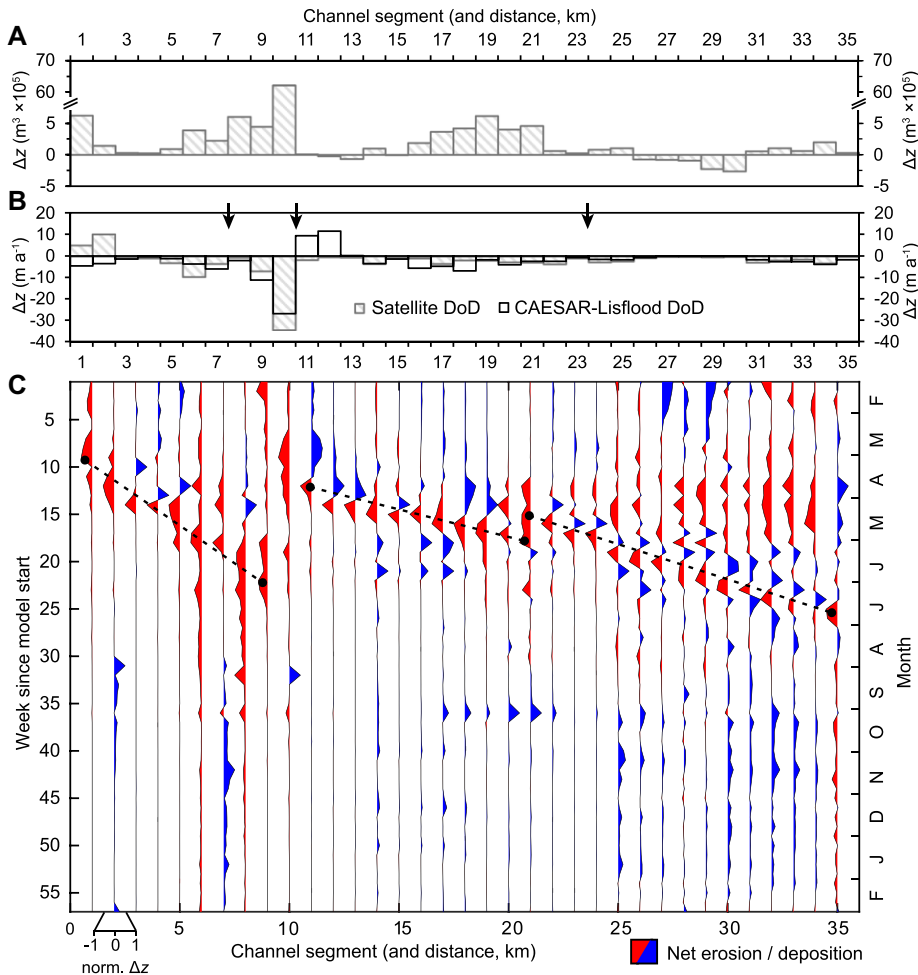


Figure 4. Spatiotemporal evolution of sediment remobilization. (A) Satellite (Pléiades) DEM of difference (DoD)–derived net surface change (Δz) September 2015–10 February 2021, caused primarily by the 7 February 2021 mass flow. **(B)** Measured (Pléiades) and modeled (CAESAR-Lisflood) Δz for the period 10 February 2021–27 January 2022. Black arrows show where CAESAR-Lisflood sub-models were coupled to one another in downstream sequence (see supplemental material [text footnote 1]). **(C)** Erosion and deposition matrix from CAESAR-Lisflood modeling, showing when and where net erosion (red) or deposition (blue) prevails within the domain at a weekly time step. Vertical lines are individual channel segments (see Fig. 1). Black dashes indicate sediment waves. To aid visualization, erosion and deposition have been normalized so that -1 and 1 are the maximum modeled erosion and deposition volume per segment.

the site of a 330 MW HPP, which exceeded pre-monsoon norms (mean 24 FNU equivalent; Sharma and Sharma, 2016) by three orders of magnitude. Turbidity reduced to an order of magnitude above pre-disturbance background values for the remainder of the pre-monsoon phase and sustained this difference through the monsoon. In April (at Batula) and June (at Srinagar), turbidity approached or exceeded that observed during the initial flood. The velocity of the post-event suspended-sediment pulse from Joshimath to Srinagar was ~ 5.7 km day^{-1} . Modeled suspended sediment yields at Joshimath were three and four orders of magnitude higher than observed pre-disturbance values for the monsoon (2014) and non-monsoon (2012, 2014) periods, respectively (Panwar et al., 2017).

DISCUSSION

Short-Term Recovery Following a Cataclysmic Perturbation

Our results indicate a fluvial system with a short relaxation time (*time taken* to recover toward a pre-disturbance state) and a relatively high degree of resilience (*ability* to recover toward a pre-disturbance state) (e.g., Pitlick, 1993; Phillips, 2009; Rathburn et al., 2018). There was an exponential decay in sediment yield in the first 12 months, indicating a high system efficiency in evacuating initially abundant sediment along with rapid incision isolating sediment deposits (cf. Adams, 1980; Major et al., 2000; Nelson and Dubé, 2016) (Fig. S4). Our observations imply a sediment exhaustion half-life of ~ 1 yr in the short-term, which is comparable with those of catchments choked

with sediment from the 1980 Mount St. Helens eruption (Washington, USA; Major et al., 2000) or the 1991 eruption of Mount Pinatubo (Philippines; Gran and Montgomery, 2005). The half-life tentatively extends to ~ 2 – 10 yr with a longer-term outlook and is sensitive to future hydrological regime (Fig. S5).

Importantly, our method of using numerical modeling to fill gaps between satellite DEM surveys reveals spatio-temporal nuances of sediment transport, including the role and speed of large-scale sediment waves. As channels affected by the Chamoli ice-rock avalanche–debris flow continue to relax, ongoing geomorphological work will be progressively restricted to being achieved by episodic flows that exceed seasonal norms (Wolman and Miller, 1960; Major et al., 2021), such as during mid-October 2021 (Fig. 3; Fig. S6).

Implications for Infrastructure, Water Quality, and Future Flood Hazard

Understanding rates and processes by which mountain fluvial systems respond to large-scale perturbations is essential for effective resource management and hazard mitigation. Extreme increases in fluvial sediment yields are detrimental for HPPs because sediment pulses can overload desilting chambers and increase the infill rate of storage reservoirs, ultimately decreasing HPP efficiency and lifetime (Li et al., 2022). Elevated sediment yields over the longer term may also need to be considered by operators of new HPPs (e.g., the 444 MW Vishnugad Pipalkoti HPP, 8.5 km downstream of Joshimath). Our modeling implies that $\sim 25\%$ of the sediment yield in the year post-event was suspended load, comprising grain fractions that are effective at damaging turbines (Singh et al., 2013). The bedload component of the modeled annual sediment yield ($\sim 75\%$) is high relative to the upper bound of bedload estimates from relatively undisturbed mountain rivers (e.g., Turowski et al., 2010) but is characteristic of a post-disturbance system with initially abundant and accessible sediment and with ample capacity for transport by seasonal high flows.

This field- and modeling-based study has characterized a high-mountain fluvial cascade that appears to be geomorphologically resilient to an extreme perturbation and that has a quantifiably short relaxation time. This system response must be understood for present and future HPPs, which are increasingly sited within high-altitude river reaches (Li et al., 2022) and are exposed to geomorphological impacts of extreme mass flows. The spatio-temporal sequencing of erosion and deposition in the form of potential “memory effects” (de Haas et al., 2020), whereby erosion is enhanced in zones of deposition in the post-flood system (and vice versa), may need to be considered in the context of future flood risk, while impacts

on aquatic ecosystems caused by the reorganization of channel substrate and modifications to nutrient load could manifest for years to decades (e.g., Danehy et al., 2011).

ACKNOWLEDGMENTS

Data involved in this research are in the process of being archived by the UKRI Environmental Information Data Centre and in the interim are available from the corresponding author on request. Westoby, Coulthard, Dunning, and Carrivick acknowledge support via the UK Natural Environment Research Council grant NE/W002930/1. Westoby and Berthier acknowledge DINAMIS/Centre National d'Études Spatiales (France) for facilitating the acquisition of Pléiades imagery. Shugar acknowledges Natural Sciences and Engineering Research Council of Canada (DG2020-0407) and Alberta Innovates. Shean and Haritashya respectively acknowledge support via NASA High-Mountain Asia grants 80NSSC20K1595 and 80NSSC19K0653, and Haritashya also acknowledges NASA Interdisciplinary Research in Earth Science grant 80NSSC18K0432 and the University of Dayton's Mann Endowed Chair in the Sciences. Sain acknowledges support from the J.C. Bose National Fellowship program (SERB-DST, New Delhi). We thank Planet Labs (San Francisco, USA) for provision of satellite data, and Shashank Bhushan for assistance with DEM generation. The authors thank the three anonymous reviewers whose comments helped to improve the manuscript.

REFERENCES CITED

- Adams, J., 1980, Contemporary uplift and erosion of the Southern Alps, New Zealand: *Geological Society of America Bulletin*, v. 91, p. 1–114, <https://doi.org/10.1130/GSAB-P2-91-1>.
- Bovis, M.J., and Jakob, M., 1999, The role of debris supply conditions in predicting debris flow activity: *Earth Surface Processes and Landforms*, v. 24, p. 1039–1054, [https://doi.org/10.1002/\(SICI\)1096-9837\(199910\)24:11<1039::AID-ESP29>3.0.CO;2-U](https://doi.org/10.1002/(SICI)1096-9837(199910)24:11<1039::AID-ESP29>3.0.CO;2-U).
- Chiarle, M., Geertsema, M., Mortara, G., and Clague, J.J., 2021, Relations between climate change and mass movement: Perspectives from the Canadian Cordillera and the European Alps: *Global and Planetary Change*, v. 202, <https://doi.org/10.1016/j.gloplacha.2021.103499>.
- Coulthard, T.J., Neal, J.C., Bates, P.D., Ramirez, J., de Almeida, G.A.M., and Hancock, G.R., 2013, Integrating the LISFLOOD-FP 2D hydrodynamic model with the CAESAR model: Implications for modelling landscape evolution: *Earth Surface Processes and Landforms*, v. 38, p. 1897–1906, <https://doi.org/10.1002/esp.3478>.
- Danehy, R.J., Bilby, R.E., Langshaw, R.B., Evans, D.M., Turner, T.R., Floyd, W.C., Schoenholtz, S.H., and Duke, S.D., 2011, Biological and water quality responses to hydrologic disturbances in third-order forested streams: *Ecology*, v. 5, p. 90–98, <https://doi.org/10.1002/eco.205>.
- de Haas, T., Nijland, W., de Jong, S.M., and McArdell, B.W., 2020, How memory effects, check dams, and channel geometry control erosion and deposition by debris flows: *Scientific Reports*, v. 10, 14024, <https://doi.org/10.1038/s41598-020-71016-8>.
- Dowling, C.A., and Santi, P.M., 2014, Debris flows and their toll on human life: A global analysis of debris-flow fatalities from 1950 to 2011: *Natural Hazards*, v. 71, p. 203–227, <https://doi.org/10.1007/s11069-013-0907-4>.
- Dutta, S., 2021, Fate of NTPC's Tapovan project hangs in balance after Rs 1,500 crore loss: *The Economic Times* (English edition), 9 February, <https://economictimes.indiatimes.com/industry/energy/power/fate-of-ntpcs-tapovan-project-hangs-in-balance-afters-1500-crore-loss/articleshow/80760066.cms>.
- Geertsema, M., et al., 2022, The 28 November 2020 landslide, tsunami, and outburst flood—A hazard cascade associated with rapid deglaciation at Elliot Creek, British Columbia, Canada: *Geophysical Research Letters*, v. 49, <https://doi.org/10.1029/2021GL096716>.
- Gran, K.B., and Montgomery, D.R., 2005, Spatial and temporal patterns in fluvial recovery following volcanic eruptions: Channel response to basin-wide sediment loading at Mount Pinatubo, Philippines: *Geological Society of America Bulletin*, v. 117, p. 195–211, <https://doi.org/10.1130/B25528.1>.
- Li, D., Lu, X., Overeem, I., Walling, D.E., Svytski, J., Kettner, A.J., Bookhagen, B., Zhou, Y., and Zhang, T., 2021, Exceptional increases in fluvial sediment fluxes in a warmer and wetter High Mountain Asia: *Science*, v. 374, <https://doi.org/10.1126/science.abi9649>.
- Li, D.F., et al., 2022, High Mountain Asia hydropower systems threatened by climate-driven landscape instability: *Nature Geoscience*, v. 15, p. 520–530, <https://doi.org/10.1038/s41561-022-00953-y>.
- Major, J.J., Pierson, T.C., Dinehart, R.L., and Costa, J.E., 2000, Sediment yield following severe volcanic disturbance—A two-decade perspective from Mount St. Helens: *Geology*, v. 28, p. 819–822, [https://doi.org/10.1130/0091-7613\(2000\)28<819:SYFSDV>2.0.CO;2](https://doi.org/10.1130/0091-7613(2000)28<819:SYFSDV>2.0.CO;2).
- Major, J.J., Spicer, K.R., and Mosbrucker, A.R., 2021, Effective hydrological events in an evolving mid-latitude mountain river system following cataclysmic disturbance—A saga of multiple influences: *Water Resources Research*, v. 57, <https://doi.org/10.1029/2019WR026851>.
- Mergili, M., Emmer, A., Juřicová, A., Cochachin, A., Fischer, J.-T., Huggel, C., and Pudasaini, S.P., 2017, How well can we simulate complex hydro-geomorphic process chains?: The 2012 multi-lake outburst flood in the Santa Cruz Valley (Cordillera Blanca, Perú): *Earth Surface Processes and Landforms*, v. 43, p. 1373–1389, <https://doi.org/10.1002/esp.4318>.
- Nelson, A., and Dubé, K., 2016, Channel response to an extreme flood and sediment pulse in a mixed bedrock and gravel-bed river: *Earth Surface Processes and Landforms*, v. 41, p. 178–195, <https://doi.org/10.1002/esp.3843>.
- Panwar, S., Agarwal, V., and Chakrapani, G.J., 2017, Morphometric and sediment source characterization of the Alaknanda river basin, headwaters of river Ganga, India: *Natural Hazards*, v. 87, p. 1649–1671, <https://doi.org/10.1007/s11069-017-2838-y>.
- Phillips, J.D., 2009, Changes, perturbations, and responses in geomorphic systems: *Progress in Physical Geography*, v. 33, p. 17–30, <https://doi.org/10.1177/0309133309103889>.
- Pitlick, J., 1993, Response and recovery of a sub-alpine stream following a catastrophic flood: *Geological Society of America Bulletin*, v. 105, p. 657–670, [https://doi.org/10.1130/0016-7606\(1993\)105<0657:RAROAS>2.3.CO;2](https://doi.org/10.1130/0016-7606(1993)105<0657:RAROAS>2.3.CO;2).
- Rathburn, S.L., Shahverdian, S.M., and Ryan, S.E., 2018, Post-disturbance sediment recovery: Implications for watershed resilience: *Geomorphology*, v. 305, p. 61–75, <https://doi.org/10.1016/j.geomorph.2017.08.039>.
- Rawat, K.S., Sahu, S.R., Singh, S.K., and Mishra, A.K., 2022, Cloudburst analysis in the Nainital district, Himalayan Region, 2021: *Discover Water*, v. 2, 12, <https://doi.org/10.1007/s43832-022-00020-y>.
- Sharma, N., and Sharma, R.C., 2016, Microbial and physico-chemical assessment of the sacred river Alaknanda at lower stretches, Uttarakhand, India: *Journal of Plant Development Sciences*, v. 8, p. 285–289.
- Shugar, D.H., et al., 2021, A massive rock and ice avalanche caused the 2021 disaster at Chamoli, Indian Himalaya: *Science*, v. 373, p. 300–306, <https://doi.org/10.1126/science.abh4455>.
- Singh, M., Banerjee, J., Patel, P.L., and Tiwari, H., 2013, Effect of silt erosion on Francis turbine: A case study of Maneri Bhali Stage-II, Uttarakhand, India: *ISH Journal of Hydraulic Engineering*, v. 19, p. 1–10, <https://doi.org/10.1080/09715010.2012.738507>.
- Stock, J., and Dietrich, W.E., 2003, Valley incision by debris flows: Evidence of a topographic signature: *Water Resources Research*, v. 39, 1089, <https://doi.org/10.1029/2001WR001057>.
- Tiwari, A., Sain, K., Kumar, A., Tiwari, J., Paul, A., Kumar, N., Haldar, C., Kumar, S., and Pandey, C.P., 2022, Potential seismic precursors and surficial dynamics of a deadly Himalayan disaster: An early warning approach: *Scientific Reports*, v. 12, 3733, <https://doi.org/10.1038/s41598-022-07491-y>.
- Toby, S.C., Duller, R.A., De Angelis, S., and Straub, K.M., 2022, Morphodynamic limits to environmental signal propagation across landscapes and into strata: *Nature Communications*, v. 13, 292, <https://doi.org/10.1038/s41467-021-27776-6>.
- Turowski, J.M., Rickenmann, D., and Dadson, S.J., 2010, The partitioning of the total sediment load of a river into suspended load and bedload: A review of empirical data: *Sedimentology*, v. 57, p. 1126–1146, <https://doi.org/10.1111/j.1365-3091.2009.01140.x>.
- UDRP-AF (Uttarakhand Disaster Recovery Project-AF), 2021, Geological and geotechnical report over Raini Village on Joshimath-Malari Road in Chamoli, Uttarakhand: Dehradun, India, Uttarakhand Disaster Recovery Project, 16 p., <http://ukdisasterrecovery.in/index.php/downloads> (accessed March 2023).
- Wolman, M.G., and Miller, J.P., 1960, Magnitude and frequency of forces in geomorphic processes: *The Journal of Geology*, v. 68, p. 54–74, <https://doi.org/10.1086/626637>.
- Zheng, G.X., et al., 2021, Increasing risk of glacial lake outburst floods from future Third Pole deglaciation: *Nature Climate Change*, v. 11, p. 411–417, <https://doi.org/10.1038/s41558-021-01028-3>.

Printed in the USA